Dose calibration of Health Canada's Fixed Point Surveillance system for environmental radiation monitoring in terms of air kerma and H*(10)

Liu, Chuanlei; Saull, Patrick R.B.; Martin-Burtart, Nicolas; Hovgaard, Jens; Korpach, Ed; Tulk, Christopher; Ungar, Kurt; Zhang, Weihua

Publisher's version / Version de l'éditeur:
https://doi.org/10.1016/j.jenvrad.2022.107009
Journal of Environmental Radioactivity, 253-254, C, 2022-09-10

Journal of Environmental Radioactivity 253-254 (2022) 107009

Contents lists available at ScienceDirect

Journal of Environmental Radioactivity

journal homepage: www.elsevier.com/locate/jenvrad

Dose calibration of Health Canada's Fixed Point Surveillance system for environmental radiation monitoring in terms of air kerma and H*(10)

Chuanlei Liu [a,*], Patrick R.B. Saull [b], Nicolas Martin-Burtart [c], Jens Hovgaard [c], Ed Korpach [a], Christopher Tulk [a], Kurt Ungar [a], Weihua Zhang [a]

[a] Radiation Protection Bureau of Health Canada, 775 Brookfield Road, Ottawa, ON, K1A 1C1, Canada
[b] Ionizing Radiation Standards, National Research Council, Ottawa, ON, K1A 0R6, Canada
[c] Radiation Solutions Inc, 5875 Whittle Road, Mississauga, ON, L4Z 2H4, Canada

ARTICLE INFO

Keywords:
Environmental radiation monitoring
Fixed pointed surveillance network
Sodium iodide detector
Dose calibration
Air kerma
Ambient dose equivalent
Linearity
Angular dependence
Accuracy

ABSTRACT

The environmental radiation exposure in Canada has been monitored since 2002 by Health Canada's Fixed Point Surveillance network. The network consists of over eighty 7.6 cm × 7.6 cm sodium iodide spectrometers, and routinely reports to the public the environmental gamma radiation level throughout Canada. This paper describes the latest dose calibrations to air kerma and ambient dose equivalent for the future upgraded network. The calibration curves were developed using Monte Carlo techniques and further optimized via experiments in various reference fields. The dose calibration was validated over a wide range of gamma energy, dose measurement range, and angle of incidence under laboratory conditions. In environmental monitoring situations, the angular distribution of radiation exposure was analytically calculated by assuming a semi-infinite plume source, semi-infinite planar source, and infinite volume sources for the respective exposure scenarios of radioactive plume, ground contamination, and soil source. By coupling the resultant radiation angular distribution with detector's angular variation on dose response, the overall accuracy of dose measurement in each of these environmental scenarios was estimated. The accuracy is expected to be within ±3.7% for plume radiation, −5.6% for ^{137}Cs ground contamination, and 0% to −17.1% for soil radioactive sources. The under-estimation for soil sources is mainly caused by absorption of radiation in the electronic system underneath the crystal.

1. Introduction

In 2002, Health Canada (HC) started to develop a countrywide network, the Fixed Point Surveillance (FPS) network, for environmental radiation monitoring and risk assessment of both the natural and anthropogenic radiation sources in Canada. At present, the network comprises over eighty 7.6 cm (diam.) x 7.6 cm thallium-doped sodium iodide [NaI(Tl)] spectrometers across the country, covering the major population centres, as well as areas in proximity to nuclear power plants and domestic ports that may berth nuclear powered vessels. More details about the FPS network and its applications can be found in [Zhang et al., 2013; Liu et al., 2018, 2019; FPS, 2021; Liu et al., 2022].

The FPS network initially employed the Exploranium GR150 NaI(Tl) detectors [Exploranium radiation detection systems, 2001], which generated spectral data in a non-linear, 512-channel format. The network has been gradually upgraded since 2008 to replace the GR150 detectors with the RS250 detectors [Radiation Solutions, 2021] from Radiation Solutions Inc. (RSI). Both detectors use the same type of crystal and photomultiplier, whereas RS250 offers a faster signal digitalization process and produces spectral data in a linear channel-energy response over 1024 channels. The current network thus works in a conversion mode that has to convert the RS250 data into GR150 format.

The hardware upgrade has been completed for years; however, the network has yet to fully benefit from it due to the outstanding tasks of upgrading the legacy GR150-dependent software as well as determining new dose conversion coefficients. Therefore, a full spectrum-dose calibration is needed in order to work directly with its spectral data without any downgrading. To this end, the Radiation Protection Bureau of HC has conducted a series of staged RS250 dose calibration measurements over the past several years by contracting BTI (Bubble Technology Industries), NRC (the National Research Council of Canada's Metrology Research Centre) and RSI. These include calibrations with X-rays, single radioisotope source (^{60}Co or ^{137}Cs), multiple radionuclide sources as shown in the experiment section of this work, and inter-comparison

* Corresponding author.
E-mail address: Chuanlei.Liu@hc-sc.gc.ca (C. Liu).

https://doi.org/10.1016/j.jenvrad.2022.107009
Received 22 July 2022; Received in revised form 22 August 2022; Accepted 1 September 2022
Available online 10 September 2022

between RS250 detectors.

In this paper, the latest RS250 dose calibration, validation, and evaluation work is presented. Specifically, the Monte Carlo (MC) method was used to derive the dose conversion curves, whereas empirical measurements were used to optimize and validate the calibration curves. The calibration accuracy has been estimated under laboratory condition and in environmental monitoring measurements. This paper aims to provide detailed information on the FPS dose calibration and its performance, and a demonstration of the compliance with international standards, as well as recommendations for stakeholders in Canada. It also supports the understanding and interpretation of the FPS dose data that are published online, found in literatures and the international organization reports, and streamed live to international radiological data exchange platforms such as the European Radiological Data Exchange Platform (EURDEP) and the international Radiation Monitoring Information System (IRMIS). Moreover, this paper could be found interesting in a broad extent to the environmental monitoring community in terms of dose calibration.

2. Dose calibration method and experiments

In this work, the RS250 detector was calibrated in terms of air kerma (K_a) and ambient dose equivalent [H*(10)] in accordance with the international recommendations [IEC 61017, 2016; ISO 4037-2, 2019]. As a fundamental physical quantity, air kerma has been secured in the FPS deliverables since the beginning. It ensures a consistent dose measurement over time and can diversify the measurement into effective dose, atmospheric radioactivity concentration, or ground deposition, if applying appropriate conversion coefficients. The newly introduced H*(10) provides a direct health impact estimation for dose control and regulatory purpose. Additionally, H*(10) harmonizes the integration of the terrestrial and cosmic [Liu et al., 2018] doses reported in FPS.

The dose calibration was conducted by RSI with the G(E) function method [Moriuchi and Miyanaga, 1966; Saito and Moriuchi, 1981, 1987]. The variable E here refers to the measured energy from RS250, and G(E) hence works as a calibration curve to derive dose directly from the measured spectrum without unfolding it. A similar method to G function but using the integrated spectral data can be found in [Ohera, 2020]. The G function can be determined by using either an experimental method [Grasty et al., 2001] or a MC technique [Yi et al., 1997; Casanovas et al., 2016; Tsuda and Saito, 2017]. In this work, a MC-based method was used.

Moreover, a series of RS250 exposure measurements were conducted at NRC in providing empirical data to optimize calibrations and validate the G(E) functions over various dose rates, energy ranges, and angles of radiation incidence.

2.1. Determination of G(E) function

To determine the G(E) functions to K_a and H*(10), Geant4 v9.4 [Hurtado et al., 2004] has been used to simulate the energy deposition of a 7.6 cm × 7.6 cm NaI(Tl) detector encapsulated in a 2-mm thick Al case. Other materials in the vicinity of the detector were omitted in the simulation. In the discrete case the G(E) function is a vector where the number of elements is equal to the number of channels in the energy spectrum. In the current RS250 configuration, a spectrum analyzer with 1024 channels is used.

A series of Geant4 simulations were performed to obtain detector responses in isotropic gamma radiation fields of 40 keV, 50 keV, 75 keV, 100 keV, 150 keV, 200 keV, 300 keV, 500 keV, 800 keV, 1000 keV, 1500 keV, 2000 keV, and 2500 keV, respectively. In each of these monoenergetic simulations, the detector response was normalized to one unit fluence, and the corresponding reference values for K_a and H*(10) were obtained based on the fluence-to-dose conversion coefficients from ICRP 74, table 21 [ICRP, 1996]. To determine the calibration coefficients for the 1024 channels with these thirteen simulation results, a least-squares fit including a penalty function on smoothness has been performed. The resulting calibration curves have been further optimized through NRC experiments in various reference fields.

2.2. Dose calibration experiments

All the dose calibration experiments were carried out at NRC in a large, low-scatter laboratory that features a high ceiling and a false aluminum floor. The RS250 detector was exposed at three different distances (1, 2 and 3 m), and several orientation angles with respect to the source. The measurements at these different distances provided detector response data for different field strengths, while the varying orientation measured the detector response in a 4-π environment. For each exposure at a fixed distance, the detector was oriented at 0° (end-on), 45°, 90° (side-on), 135° and 160° from the source with respect to its symmetry axis. Fig. 1 illustrates an end-on experiment setup where the detector was raised about 40 cm above its aluminum support table by polystyrene foam to minimize scatter contributions from the platform. The radioactive source is positioned on another sliding platform outside the field of view, to the left, and at the same height as the detector.

Eight liquid radionuclide sources, flame-sealed into NIST ampoules (~5 ml), were used in these experiments. The activity of each source was determined at NRC using primary-standard 4π beta-gamma (anti)coincidence counting and secondary-standard ionization chamber measurements. Detailed information including radionuclide activities, predominant photon energies and their emission rates is given in Table 1.

The reference dose rates at different distances were derived by NRC from the measured source activity using EGSnrc Monte Carlo simulations [Kawrakow et al., 2017]. Isotropic gamma emissions were simulated as originating uniformly from a 5 ml volume of water contained within a borosilicate-glass cylinder of 1.65 cm outer diameter, 4.0 cm height, and 0.6 mm wall thickness. These were transported out of the ampoule and to the detector position in an efficient manner using variance-reduction techniques. The air, walls, false floor, and support tables and platforms were all included in the simulation to account for scattering and absorption contributions to the derived air-kerma rate. This was scored in an air sphere of radius 5 cm located at the detector position (taken to be the geometric centre of the crystal), where the photon fluence as a function of energy was also scored for the H*(10) calculation.

The reference dose rates obtained this way were confirmed at NRC through direct measurement of the air-kerma rate using a 15-L Exradin A8 ionization chamber in the field of the strong ^{60}Co source. The values agreed within 1%, thus validating the approach.

Fig. 1. Set up for an end-on calibration carried out at NRC. The RS250 detector is placed on 40 cm thick polystyrene foam and the irradiation source is positioned to the left of the detector outside the field of view.

Table 1
The radionuclide sources used for calibration experiments at NRC. In each radionuclide case, only these predominant photon emissions (at least greater than 1%) are shown.

Source	Activity [MBq]	Gamma-rays		X -rays	
		Energy [keV]	Emission prob.	Energy [keV]	Emission prob.
^{241}Am	59.9 ± 0.2%	26.3, 59.5	2.31%, 35.92%	11.9–22.2	37.66%
^{57}Co	197.5 ± 0.4%	122.1, 136.5	85.51%, 10.71%	6.4–7.1	57.10%
^{51}Cr	632.0 ± 2.0%	320.1	9.89%	4.9–5.5	22.84%
^{137}Cs	3.24 ± 0.5%	661.7	84.99%	31.8–37.4	6.84%
^{60}Co (strong)	33.8 ± 0.2%	1173.2, 1332.5	99.85%, 99.98%	7.5–8.3	<0.01%
^{60}Co (weak)	1.41 ± 0.3%	1173.2, 1332.5	99.85%, 99.98%	7.5–8.3	<0.01%
^{88}Y	35.4 ± 1.0%	898.0, 1836.1	93.70%, 99.35%	14.1–16.1	60.66%
^{24}Na	60.2 ± 0.3%	1368.6, 2754.0	99.99%, 99.86%	–	–

The background radiation in the NRC laboratory was measured during several relatively stable periods over the course of the tests. For an exposure within a specified period, the average background measured for that period was used to correct the reported RS250 dose rates prior to comparison with the reference dose rates.

3. Results and discussions

3.1. G(E) calibration curves

The spectrum-dose calibration curves obtained in this work are shown in Fig. 2; one for air kerma and the other for H*(10). Both curves have a "check mark" shape: decreasing in the low energy range, attaining the minimum at around 60 keV, and increasing afterwards. These characteristic shapes represent a combined behavior of the energy-dependent NaI(Tl) intrinsic detection efficiency ($\varepsilon(E_0)$) and gamma mass energy-transfer coefficients ($\mu_{tr}(E_0)/\rho$) in air and tissue, and the effect of ICRU 4-element sphere phantom. Here E_0 refers to the incident gamma energy, whereas the energy in the figure refers to the measured energy from RS250.

Air kerma can be defined as $K_a = \Phi \cdot E_0 \cdot (\mu_{tr}(E_0)/\rho)$. The coefficients $\mu_{tr}(E_0)/\rho$ in air and tissue decrease from 1 keV to 60 keV by about 5 orders of magnitude, and tend to flatten beyond 60 keV and up to 20 MeV with a variation level within a factor of 2–3. After coupling $\mu_{tr}(E_0)/\rho$ with its E_0, K_a/Φ then gets a similar "check mark" shape as the one seen in Fig. 2. Even though that shape is based on E_0 and per fluence (Φ), it is the underlying reason of the air kerma G(E) shape found here in Fig. 2. This is the same for the H*(10) G(E) curve, which is additionally subject to the attenuation effect of photons in the ICRU sphere.

The calibration curves in Fig. 2 are in terms of count rate and measured energy E. These are the modified shapes of the K_a/Φ and H*(10)/Φ after considering the varying $\varepsilon(E_0)$ that connects Φ at E_0 and the count rate at E.

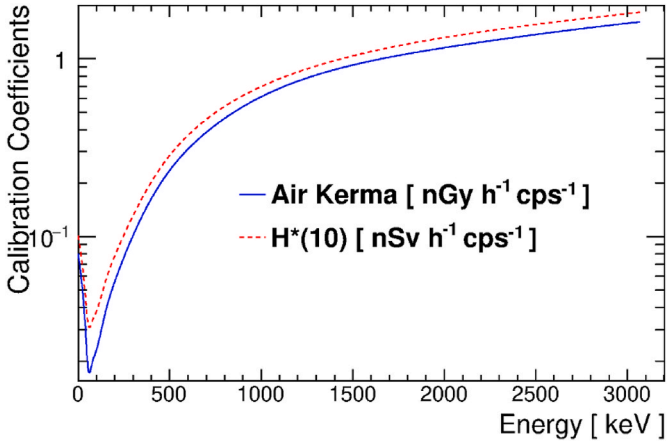

Fig. 2. The RSI calibration curves, G(E)s, to convert the RS250 count rate to dose rates.

3.2. NRC experiments

A series of calibration spectra that were measured at NRC are shown in Fig. 3. These spectra are from a side-on exposure scenario at 1 m distance and prior to background radiation subtraction. As implied by the characteristic gamma peaks, the radionuclides used in experiments cover an energy range from 59.5 keV to ~3 MeV.

As an environmental dosimeter, RS250 is designed to provide dose measurement on the strongly penetrating gamma radiation that has energies above 15–20 keV. In practice, the RS250 response to gammas below this level is considerably suppressed by the detector dead material such as the aluminum housing case. This aluminum case has a slightly increased thickness from the top to the bottom end with an average thickness at a fraction of cm level. Theoretical calculations show that, for a 0.2 cm thick aluminum case, about 99% of photons of 15 keV will be attenuated while 54% of 30 keV photons can transmit through. Additionally, the presence of the electronics and the supporting pole below the crystal can also largely affect the detection of gamma rays incident from below, especially at low energy.

Experimentally, a close-up examination of the low-energy regions of the ^{137}Cs and ^{241}Am spectra, as low as at ~20 keV, has been conducted. As shown in Fig. 4, the ^{137}Cs X-ray peak is clearly seen at the corresponding energy range from 31.8 to 37.4 keV (Table 1) with a count rate comparable to the characteristic gamma-ray peak at 662 keV. Therefore, the ^{137}Cs calibration result can be indicative of the G(E) performance down to 30 keV. The response at lower energy region can also be checked by using the ^{241}Am spectrum as presented in Fig. 4. Besides the 59.5 keV peak, this spectrum displays a convolved peak of the iodine X-ray escape peak at 31.5 keV, the ^{241}Am 26.3 keV gammas, and multiple X-rays of ^{241}Am ranging from 11.9 to 22.2 keV. No intention was made to separate or quantify each of these peaks in this work. Instead, by

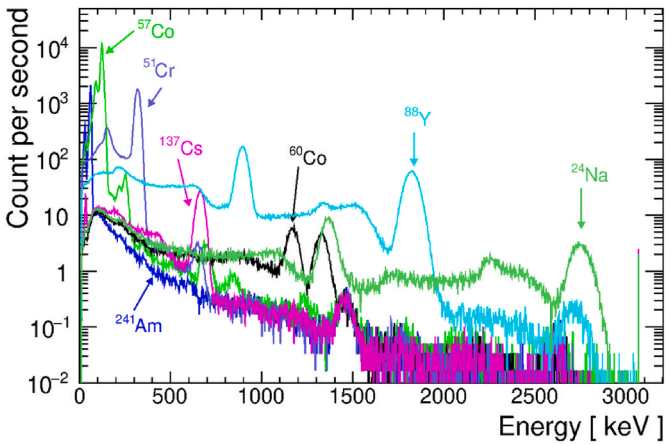

Fig. 3. A series of side-on calibration spectra measured at NRC.

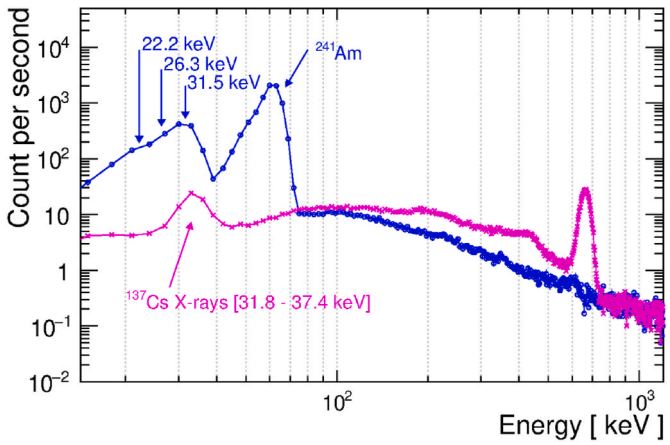

Fig. 4. The ^{137}Cs and ^{241}Am spectra used to demonstrate the low energy feature.

showcasing this count enriched region, the performance of the RSI calibration in the photon energy region down to ~20 keV can be tested and verified.

3.3. Validation of the dose calibration

The measured dose in RS250, hereafter referred to as the RS250 dose, is calculated by integrating the G(E) weighed energy spectrum over an energy range from a specified cut-off value up to 3 MeV. The RS250 dose rate is then given by the quotient of the RS250 dose by the measurement time, denoted by $\dot{K}_a$ for air kerma rate and $\dot{H}^*(10)$ for the ambient dose equivalent rate. The existence of a cut-off value here reflects the realistic constraints of the RS250 detector in response to low-energy photons, and is also in compliance with the low energy limit of the H*(10) measurement. Two cut-off values at 18 keV and 30 keV were tested in this study. Accordingly, at each cut-off scenario, NRC provides traceable activity-based reference dose rates.

The RS250 dose rate, $\dot{K}_a$ or $\dot{H}^*(10)$, and its deviation relative to the NRC reference dose rate are provided in Tables 2 and 3 for the 30 keV and 18 keV cut-off scenarios, respectively. All results were obtained from a side-on exposure scenario at 1 m distance and with background subtracted. The uncertainty of the RS250 dose rate is derived from the spectral data and account for statistical fluctuation only. The uncertainty on the NRC reference rate, on the other hand, is a combined uncertainty out of EGSnrc simulation statistics, activity uncertainty, and uncertainties in the detector/crystal positioning with respect to the source.

The relative deviations shown in Tables 2 and 3 are defined as (RS250-Ref)/Ref, and all results are found to be consistent with zero within three standard deviations. In the case of the 30 keV cut-off scenario, the largest deviation is found in the ^{51}Cr $\dot{H}^*(10)$ result at (3.77 ± 2.38)%. Another large discrepancy can be seen in the ^{137}Cs results where the RS250 dose rates are under-estimated by 1.66%–2.67% against the NRC references. However, owing to the large uncertainty (mainly from the ^{51}Cr activity uncertainty) associated with the deviation result, the RS250 detector is still considered to be well calibrated in this specific case.

With a lower cut-off threshold at 18 keV, the RS250 dose rates were recalculated and compared with the NRC references obtained with the same cut-off energy. The corresponding results, as seen in Table 3, show a similar level of deviation as found in Table 2 where the 30 keV cut-off is applied. The ^{51}Cr $\dot{H}^*(10)$ deviation is found to be still high at (4.35 ± 2.39)%.

All results, conservatively speaking, suggest that the RS250 dose response can be calibrated within 4.35% to both K_a and H*(10) dose rates in reference to the NRC reference rates.

3.4. $\dot{H}^*(10)/\dot{K}_a$ or h_K ratios

The performance of the dose calibration was further examined by comparing the RS250 h_K ratio (i.e., $H^*(10)/K_a$) with the reference ratios from NRC and ICRP/ISO [ICRU, 1992; ISO 4037-3, 2019]. This was done in the 30 keV cutoff scenario where both the RS250 ratios and the NRC reference ratios are calculated directly from the dose rates given in Table 2. The ICRP ratio, on the other hand, is calculated based on the H*(10) and K_a values, which are derived for each radionuclide by summing the products of gamma ray intensity and the respective ICRP dose/Φ coefficient over all gammas of the radionuclide in consideration. The comparison is shown in Fig. 5. Note that the energy in x-axis is defined simply as either the average gamma energy of a radionuclide (e.g. ^{60}Co) or the highest energy of the characteristic gammas for illustrative purpose.

In comparison to the ICRP (NRC) references, the RS250 h_K ratios agree well within 1.5% for all radionuclides except for the ^{241}Am result, where RS250 h_K is 3.5% (2.9%) lower. One possible reason to explain the discrepancy in ^{241}Am can be related to the accuracy of the RSI calibration curves in the energy region represented by the ^{241}Am 59.5 keV and below. As seen in Fig. 4, rich and intense spectral features exist at energies ranging from 20 to ~30 keV in the ^{241}Am spectrum. These features can be directly related to the ^{241}Am photons in that energy range, as given in Table 1, or due to the iodine X-ray escape process in NaI. Moreover, the RSI G(E) curves are derived based on thirteen calibration points, and extrapolation was made to extend the energy region below the least energy point at 40 keV in simulation. Therefore, it is plausible that the current RSI calibration at energies below 40 keV could be not sufficiently accurate for the ^{241}Am dose estimation where the low energy region is relatively important.

Nevertheless, owing to the overall good performance found in the energy range from 18 keV to 3 MeV, the RS250 detector can be considered well calibrated within an accuracy of 4.35% for both air kerma and ambient dose equivalent rates under a laboratory condition. Practically, a well validated calibration down to 18 keV can support the future use of typical Xenon X-rays to enhance the dose measurement that

Table 2
The RS250 dose rates and their relative deviations from the NRC reference rates. These results are obtained for a side-on exposure scenario with a cut-off value of 30 keV. ^{60}Co(a) and ^{60}Co(b) refer to the weak and strong ^{60}Co sources, respectively.

	Air Kerma Rate (nGy/h)			Ambient Dose Equivalent Rate (nSv/h)		
	RS250 $\dot{K}_a$	NRC ref $\dot{K}_a$	Rel. Deviation (%)	RS250 $\dot{H}^*(10)$	NRC ref $\dot{H}^*(10)$	Rel. Deviation (%)
^{241}Am	200.45 ± 1.25	197.88 ± 2.27	**1.30 ± 1.33**	336.37 ± 1.48	341.57 ± 3.88	**−1.52 ± 1.20**
^{57}Co	2575.32 ± 1.83	2533.74 ± 30.36	**1.64 ± 1.22**	4038.19 ± 2.42	3945.84 ± 46.90	**2.34 ± 1.22**
^{51}Cr	3035.91 ± 2.61	2946.28 ± 67.64	**3.04 ± 2.37**	3975.58 ± 3.29	3831.10 ± 87.80	**3.77 ± 2.38**
^{137}Cs	237.63 ± 1.63	244.16 ± 3.01	**−2.67 ± 1.37**	289.56 ± 1.92	294.46 ± 3.61	**−1.66 ± 1.37**
^{60}Co(a)	348.23 ± 2.26	348.76 ± 4.06	**−0.15 ± 0.65**	401.97 ± 2.58	397.36 ± 4.64	**1.16 ± 1.34**
^{60}Co(b)	9001.87 ± 9.84	8917.13 ± 101.94	**0.95 ± 1.16**	10383.99 ± 11.19	10159.80 ± 115.47	**2.21 ± 1.17**
^{88}Y	7974.23 ± 9.89	8109.74 ± 122.29	**−1.67 ± 1.49**	9234.09 ± 11.30	9337.93 ± 140.14	**−1.11 ± 1.49**
^{24}Na	969.36 ± 4.20	971.93 ± 11.33	**−0.26 ± 1.24**	1110.05 ± 4.78	1098.18 ± 12.72	**1.08 ± 1.25**

Table 3
The RS250 dose rates and their relative deviations from the NRC reference rates. These results are obtained for a side-on exposure scenario with a cut-off value of 18 keV.^{60}Co(a) and^{60}Co(b) refer to the weak and strong^{60}Co sources, respectively.

	Air Kerma Rate (nGy/h)			Ambient Dose Equivalent Rate (nSv/h)		
	RS250 $\dot{K}_a$	NRC ref $\dot{K}_a$	Rel. Deviation (%)	RS250 $\dot{H}^*(10)$	NRC ref $\dot{H}^*(10)$	Rel. Deviation (%)
^{241}Am	223.74 ± 1.26	227.45 ± 2.61	**−1.63 ± 1.26**	367.55 ± 1.49	368.92 ± 4.19	**−0.37 ± 1.20**
^{57}Co	2597.31 ± 1.83	2530.76 ± 30.32	**2.63 ± 1.23**	4067.49 ± 2.42	3945.31 ± 46.89	**3.10 ± 1.23**
^{51}Cr	3052.71 ± 2.61	2946.05 ± 67.63	**3.62 ± 2.38**	3997.94 ± 3.29	3831.44 ± 87.81	**4.35 ± 2.39**
^{137}Cs	238.26 ± 1.63	244.23 ± 3.01	**−2.44 ± 1.38**	290.41 ± 1.92	294.73 ± 3.61	**−1.47 ± 1.37**
^{60}Co (a)	348.53 ± 2.26	348.74 ± 4.06	**−0.06 ± 1.33**	402.37 ± 2.58	397.45 ± 4.65	**1.24 ± 1.34**
^{60}Co(b)	9009.89 ± 9.84	8916.49 ± 101.94	**1.05 ± 1.16**	10394.66 ± 11.19	10162.20 ± 115.50	**2.29 ± 1.17**
^{88}Y	7981.19 ± 9.89	8118.37 ± 122.42	**−1.69 ± 1.49**	9243.35 ± 11.30	9337.58 ± 140.14	**−1.01 ± 1.49**
^{24}Na	969.80 ± 4.20	971.74 ± 11.33	**−0.20 ± 1.24**	1110.64 ± 4.78	1098.03 ± 12.72	**1.15 ± 1.25**

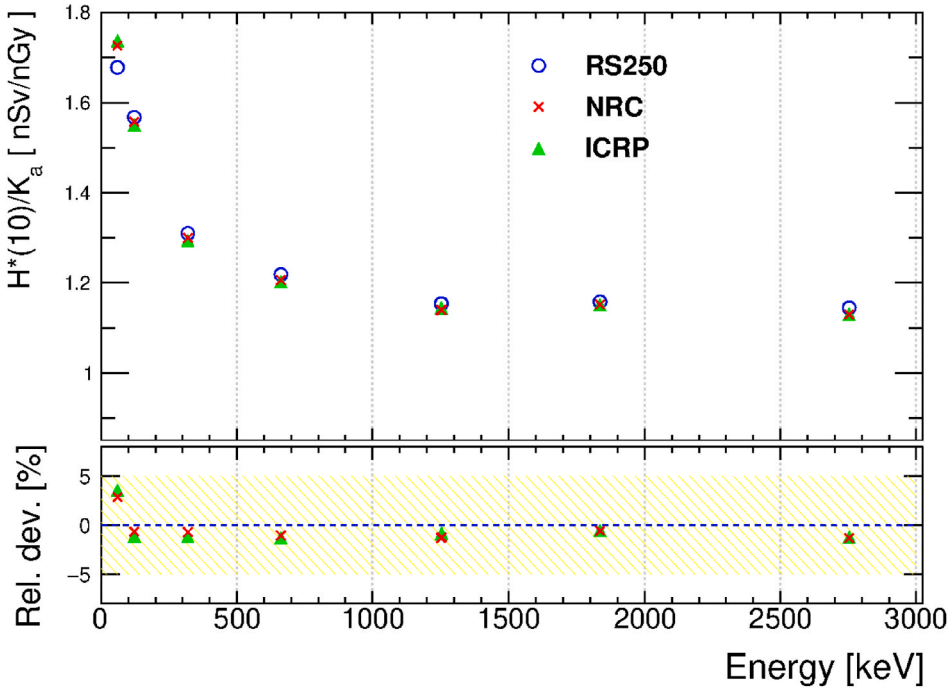

Fig. 5. The $H^*(10)/K_a$ ratios obtained from RS250 responses, NRC and ICRP reference values. Here the energy on the X-axis is given by either the averaged gamma energy (i.e. ^{60}Co) or the highest gamma energy given in Table 1 (e.g. ^{88}Y and ^{24}Na).

was usually obtained with characteristic gamma rays only.

3.5. Linearity

The discussions so far are only for the side-on exposure at 1 m distance. To check the linearity of the detector response in different dose rate ranges, a series of experiments has been conducted at three different source-detector distances. Among these experiments, the lowest dose rates (25 nGy/h) are found in the case of ^{241}Am and ^{137}Cs exposures at 3-m distance. This level of exposure is close to the averaged terrestrial radiation in Canada (25 nSv/h) [Grasty and LaMarre, 2004]. The maximum dose rate, on the other hand, is obtained from the strong ^{60}Co source at a level of 10 μGy/h. This calibration range generally complies with the IEC standard on the effective measurement range of 30 nGy/h to 30 μGy/h for an area dosimeter [IEC 61017, 2016].

As Fig. 6 illustrates, the detector response to air kerma has a very good linearity within 5% over the full dose rate range and over a photon energy range above the ^{241}Am gamma line. For ^{241}Am, the RS250 dose rate tends to underestimate the NRC reference rate as the dose rate decreases (or, experimentally, as the source-detector distance increases). Specifically at the lowest dose rate of ~25 nGy/h, the RS250 is about 8% lower than the NRC reference rate, even though it is not

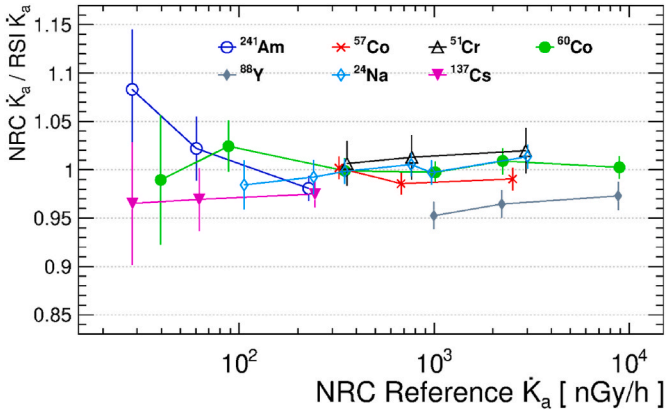

Fig. 6. Linearity of the RS250 response to air kerma rate at various dose rates.

statistically significant by considering its associated uncertainty. The overall trend found in ^{241}Am seems to be related to the increasing attenuation effect of low-energy photons in air as the source-detector distance increases. This effect is particularly important for ^{241}Am

because of the large abundance of low-energy photon emissions with respect to its characteristic gamma-rays, as seen in Table 1. The possible difference in treating this effect between NRC and RSI can be the cause of this trend found in ^{241}Am.

Furthermore, fifteen RS252 detectors have been calibrated with high ^{137}Cs dose exposure at Stuart Hunt & Associate Ltd. in 2014. The RS252 detector is a portable version of RS250, and the main difference between them is the amount of materials underneath the detector due to the change in mounting configuration and electronics position. The exposure was conducted in the side-on scenario with dose rates ranging from 2 μSv/h to 200 μSv/h, representing a dose range found in routine monitoring near nuclear power plants or in a nuclear emergency situation. Two of the fifteen detectors are excluded in this work because they are suspected to have either crystal shift or some electronic problems. For the remaining detectors, the linearity of dose responses are within −1%–12%. This result can well represent the linearity of the RS250 detector because no difference is expected on the dose response of two detectors in this source-detector orientation.

3.6. Angular variation of the response

All RS250s deployed to the field are mounted on an aluminum post and pointing upwards to the sky, as illustrated in Fig. 7. As a result, each has field of view coverage of nearly 4π steradian. The end-on radiation discussed previously refers to a polar angle (θ) of zero degrees in the spherical coordinates. In this coordinate system, the airborne plume and cosmic radiation mainly come from 0° to π/2, whereas the radiation from the ground and soil largely from π/2 to π.

All the empirical results discussed previously are in a fixed direction exposure scenario and in a laboratory condition. To adapt for environmental monitoring measurements, the RS250 angular response to dose

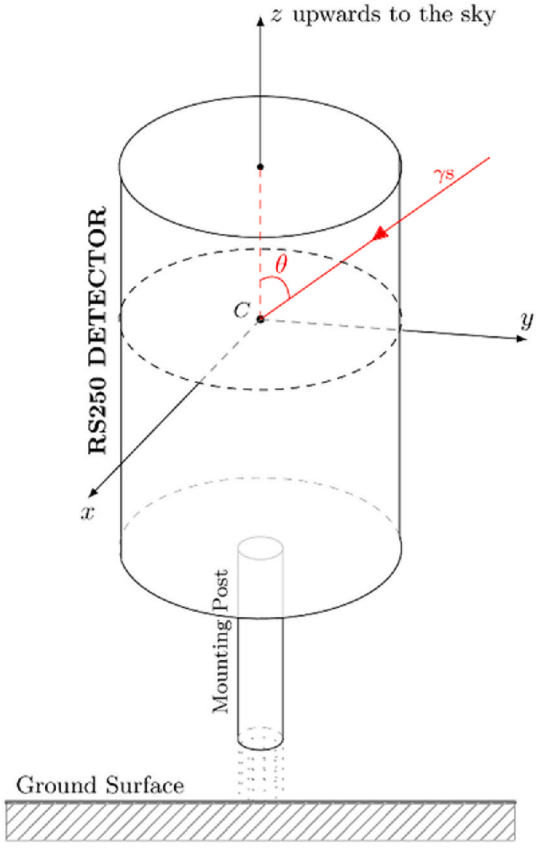

Fig. 7. Schematic diagram of RS250 deployment in field and the definition of the polar angle θ.

rate has been checked. The detector was exposed at four specific orientation angles (i.e., θs) of 0°, 45°, 135° and 160° with respect to the radiation source. For each irradiating source, it was sustained at a fixed distance from the geometric centre of the 7.6 cm × 7.6 cm crystal in all orientations such that the nominal dose rate was the same. This nominal value was represented by the RS250 dose rate obtained in side-on (90°) exposure, to which exposures in other orientations are normalized. The normalization gives a set of dose ratios, indicative of the detector response variation solely due to orientation. In Table 4 and Fig. 8, the $\dot{K}_a$ ratios at different orientation scenarios are presented.

In the 45° incident scenario, for example, the detector response is found to be, at most, by ~9% higher than the side-on result after applying the same calibration curves given in Fig. 2. For high energy photons in the same incident angle, no considerable difference is found on detector response in comparison to the 90° results. In an extreme case of the overhead exposure (0°), RS250 tends to produce a $\dot{K}_a$ result that is lower by 7–18% with respect to the side-on measurement over the full energy range.

In reality, plume can be present in different forms, sizes, heights, and incident directions. Therefore, for an environmental dosimeter with a varying angular response such as RS250, it is challenging to have a dose measurement as accurate as reported in the side-on experiment without knowing its geometry and gamma compositions. As a good practice, a plume model is usually assumed in calibrating an area dosimeter and estimating dose. As suggested by the empirical [Grasty et al., 2001] and simulated results [ICRP, 2020], a homogeneous semi-infinite plume source can be created from a combination of weighed dose responses at different incident angles from 0° to 90° (or to 180° if the ground scattering is considered). By assuming a cosine dependence of the fluence on polar angle (θ), the fluence weighting factors (*f*s) can be estimated by using formula $f(\Delta\theta) = \cos(\theta_2)\text{-}\cos(\theta_1)$ between two angles θ_1 and θ_2. For the orientation range as shown in Table 4, these *f*s are 0.07612, 0.5412 and 0.3827 for Δθs of 0°-to-22.5°, 22.5°-to-67.5°, and 67.5°-to-90°, respectively. Then the overall accuracy (*A*) of $\dot{K}_a$ for plume exposure can be calculated from the sum of *f*-weighted accuracies in various angular ranges; it is expressed as $A = W_{ref} \cdot \sum f(\Delta\theta) \cdot [R(\Delta\theta)\text{-}1]$. Here $R(\Delta\theta)$ is the $\dot{K}_a$ ratios shown in Table 4, and W_{ref} is a correction factor accounting for the dose accuracy of the reference direction (i.e., ±4.35% from side-on results). To have a conservative estimation of *A*, W_{ref} is set to 1.0435. A simple calculation then implies that, the RS250 dose calibration has a $\dot{K}_a$ bias of $A = 3.7\%$ for ^{241}Am plume, and $A = -1.7\%$ for ^{24}Na plume. These calculations suggest that the RS250 dose calibration is able to provide plume dose measurement within 3.7% accuracy based on a semi-infinite plume model.

For ground surface contamination and the NORM radiation in soil, the RS250 dose can be approximated by assuming an infinite planar source and an infinite volume source [Isaksson, 2011; ISO 18589-7, 2013; ICRP, 2020], respectively. To get $f(\Delta\theta)$ in both cases, the angular dependence of the fluence is analytically calculated based on [Isaksson, 2011]. Furthermore, the $R(\Delta\theta)$s in Table 4, and the angular intervals of 90°-to-112.5°, 112.5°-to-147.5° and 147.5°-to-180° are used for estimating *A* in both environmental situations. As shown in Table 4,

Table 4
The angular variation of the RS250 response ($\dot{K}_a$) with respect to the same radiation exposure. The air kerma rate in each angular exposure situation is normalized to the $\dot{K}_a$ result in 90°.

Source	0°	45°	90°	135°	160°
Am-241	0.82 ± 0.01	1.09 ± 0.02	1.00	0.66 ± 0.02	0.22 ± 0.03
Co-57	0.83 ± 0.01	1.09 ± 0.02	1.00	0.91 ± 0.01	0.48 ± 0.01
Cr-51	0.85 ± 0.01	1.01 ± 0.01	1.00	0.92 ± 0.01	0.61 ± 0.01
Cs-137	0.89 ± 0.02	0.98 ± 0.03	1.00	0.89 ± 0.02	0.66 ± 0.02
Co-60	0.93 ± 0.01	1.01 ± 0.02	1.00	0.95 ± 0.02	0.78 ± 0.01
Y-88	0.93 ± 0.01	0.99 ± 0.01	1.00	0.94 ± 0.01	0.77 ± 0.01
Na-24	0.93 ± 0.01	0.98 ± 0.02	1.00	0.93 ± 0.02	0.80 ± 0.02

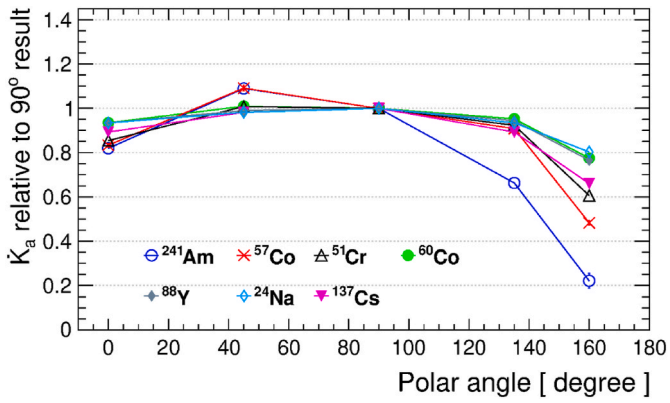

Fig. 8. The angular variation of the detector reported air kerma rate as a function of polar angle. The Y-axis shows the ratio of the air kerma rate result in each polar angle for multiple radionuclides.

large underestimation of the dose is found for RS250 response at 160° exposure. This is due to the presence of the enclosed electronics and the housing case below the NaI crystal. Such impact can be well within the acceptable limit in an actual ground deposition exposure, especially the case of surface and shallow deposition of nuclear fallout. This is because the dose contribution under RS250 is relative small, for example, only about 6% between polar angle of 140° −180° [Isaksson, 2011; Tsuda and Saito, 2017]. In the case of ^{241}Am ground deposition, RS250 can underestimate dose by ~17.0%. The accuracy improves as radiation energy increases, and it becomes ~5.6% for ^{137}Cs ground contamination.

For the NORM concentration in soil, the evaluation of *A* becomes complicated because of the soil attenuation effect. The attenuation modifies not only the energy spectrum, but also the directional distribution of the radiation reaching RS250. The extent of the impact is also subject to the soil depth and the gamma energy of NORM radionuclides, which have a broad range from several hundred keV to 2.6 MeV. For these un-scattered radiation, its angular distribution above ground can be either analytically estimated [Beck et al., 1972; Isaksson, 2011] or calculated with MC simulations [ICRP, 2020]. The analytical method is used in this work by assuming an infinite volume source with uniformly distributed NORM radionuclides in soil. The results show that as the depth increases, the proportion of un-scattered photons from that depth will considerably decrease and their directions will tend toward upwards to the ground [ICRP, 2020]. However, most of un-scattered photons comes from the very top few cm of the soil (e.g, 50% of gammas at the ^{137}Cs energy level are from top 2–3 cm of soil). Therefore, the overall direction of un-scattered photons is still pronounced from a direction tens of degrees away from vertical. For example, about 75% of radiation flux comes from the direction of 100° −150° (or from an area bounded by radii of 0.6 m–5.7 m) for RS250 at 1 m height above the ground. The overall shape is more or less similar for all major gammas from NORM radionuclides. To be conservative, the angular variation of ^{137}Cs in Table 4 is used. This is because its gamma energy is close to the major low energy NORM gammas, which has a poor dose response in comparison with MeV NORM gammas. After applying $f(\Delta\theta)$s to the aforementioned angle intervals, RS250 dose is about −17.1% lower than the expected dose for the un-scattered gammas.

For these attenuated photons that originate from soil, their directional distribution is nearly isotropic, slightly enriched in the lateral direction [Tsuda and Saito, 2017]. Note that the scattered photons usually have a lower energy than these un-scattered photons. These scatted photons can arrive either from above the detector (i.e., downward incidence with polar angle less than 90°) or below the detector (i.e., upward incidence with a θ greater than 90°). For downward incident photons, they are unlikely to cause large bias, as implied from the small *A* found in the semi-infinite plume results. For these upward incident photons, a similar infinite plane as used in the ground deposition study is assumed to calculate *A*. Again, to be conservative, the ^{241}Am ground deposition results are used here, in which RS250 underestimates dose by A = -17.0%. For a realistic exposure scenario arising from soil radionuclides, *A* should be a weighted combination of these three cases (i.e., un-scattered, downward- and upward-incidence). The weighting factors in three cases vary depending on the actual radiation situation. Nevertheless, the overall accuracy *A* from NORM radionuclides in soil should be close to, or better than, the conservative estimation here: ~17.1%.

3.7. Conformity to international standards in terms of accuracy

The dose calibration in this work followed the international standards and/or guidance in terms calibration procedure, such as reference sources [ISO 4037–1, 2019], and the operational dose quantities and dose conversion coefficients [ICRU, 1992, 2020; ICRP, 2020]. The calibration has been further evaluated in terms of the accuracy of the RS250 dose measurements. This was done in sections 3-6 relative to either the reference dose rate in a laboratory condition, or to the analytical dose rate in environmental monitoring. The evaluation aims to ensure the compliance of the RS250 dose calibration with the related international standards/requirements. These standards are made regarding the linearity of the dose measurement range, dose response variation with photon energy, angular variation [IEC 61017, 2016; IEC 60532, 2010], and the overall dose accuracy as an environmental dose monitor [ICRU, 1992; ICRP, 1997]. All accuracies considered in this study comply with the IEC, ICRU and ICRP limits, as listed in Table 5. Except for the variation of response with angle of incidence, all other limits and RS250 accuracy results presented in this table are the absolute dose responses. The angular variation is expressed as a relative response with respect to the response at zero degrees angle of incidence.

3.8. Application of the calibration curves across FPS network

Prior to implementing the calibration curves to the whole FPS network, detector-to-detector variation has been taken into account. The variations could be due to either physical or software configuration (i.e. in construction and/or assembly or software optimization).

Three randomly selected RS250 detectors, representative of the entire network, were exposed to radiation fields at BTI in 2013. A ^{137}Cs reference source at 17 MBq was used at different distances and two different detector orientations. The inter-comparison results show that the precision of all three detector responses, defined as the standard

Table 5
Conformity of the RS250 dose measurement accuracy with international standards or requirements.

Characteristic/ quantity	Standard limits	RS250 accuracy
Linearity	IEC 60532:2010; < ±30%	−5% to +8% @ 25 nGy/h to 10 μGy/h
	IEC 61017:2016; −15% to +22% @ 30 nGy/h to 30 μGy/h	−1% to +12% @^{137}Cs: 2 μSv/h to 200 μSv/h
Variation with energy	IEC 60532:2010; −25% to +40% between 80 keV and 1.5 MeV	< ±4% @ 60 keV to 2.75 MeV
	IEC 61017:2016; < ±30% between 80 keV and 1.5 MeV	
Angular variation[a]	IEC 61017:2016; ±20% @^{137}Cs between 0° to ±120°	0%–12% @^{137}Cs between 0° to 135°
Overall dose accuracy	ICRU 47: 1992; <±30% @ 1 standard deviation.	Plume < ±3.7%
	ICRP 75:1997; 1.5 times @ 95% confidence level	Surficial contamination:−5.6% @^{137}Cs NORM: 0% to −17.1%

[a] Note the RS250 0° (end-on) dose rate is used as the reference to normalize dose rates at other angles for the RS250 angular accuracy results in this table.

deviation divided by the average, ranges from a fraction of % to ~1% in all exposure scenarios. Additionally, the RS252 calibrations mentioned in section 4 show that the response difference among all thirteen detectors are within 1% for dose rate range below 10 μSv/h. The difference increases as the exposure dose rate rises, and it can be up to 6% at 200 μSv/h.

4. Summary

This paper describes the latest dose calibration work pertaining to Health Canada's upgraded Fixed Point Surveillance network. Through a joint effort with RSI and NRC, the RS250 detector has been calibrated to air kerma and ambient dose equivalent. The calibration curves were obtained based on RSI simulation results and further tuned with NRC experiments.

The results show that the RS250 dose measurement has been calibrated within an accuracy of ±4.35% in an energy range from 18 keV to 3 MeV, and −5% to +12% over a dose rate range of four orders of magnitude. The RS250 detector exhibits variable angular response due to its cylindrical geometry, the aluminum housing, and the electronic material under the crystal.

In environmental monitoring, the angular distribution of radiation fluence was analytically calculated by assuming a semi-infinite plume source, semi-infinite planar source, and infinite volume sources for the respective exposure scenarios of radioactive plume, ground contamination, and soil source. By coupling angular fluence distribution with angular variation of the RS250 dose response, the overall accuracy of RS250 dose measurement in each of these scenarios was estimated. The accuracy is expected to be within ±3.7% for plume radiation, −5.6% for ^{137}Cs ground contamination, and 0% to −17.1% for soil sources. The under-estimation for soil sources is primarily caused by absorption of radiation in the electronic system underneath the crystal. Either a new set of calibration coefficients for that area, or simply a correction factor on the current calibrations can be applied to remedy this effect.

Declaration of competing interest

The authors declare that they have no known competing financial interests or personal relationships that could have appeared to influence the work reported in this paper.

Data availability

Data will be made available on request.

References

Beck, H.L., DeCampo, J., Gogolak, C., 1972. In Situ Ge(Li) and Nai(Tl) Gamma-Ray Spectrometry. https://doi.org/10.2172/4599415. NSA-27-000357, United States. Web.

Casanovas, R., et al., 2016. Calculation of the ambient dose equivalent H*(10) from gamma-ray spectra obtained with scintillation detectors. Appl. Radiat. Isot. 118, 154–159.

Exploranium radiation detection systems, 2001. GR-150 Perimeter Radiation Monitoring System for Ontario Power Generation. Part#26018-1 Rev.7, July 2001.

FPS, 2021. The FPS Website at Health Canada. https://www.canada.ca/en/health-canada/services/health-risks-safety/radiation/understanding/measurements.html.

Grasty, R.L., et al., 2001. Calibration of a 7.6 cm x 7.6 cm (3 inch x 3 inch) sodium iodide gamma ray spectrometer for air kerma rate. Radiat. Protect. Dosim. 94 (4), 309–316.

Grasty, R.L., LaMarre, J.R., 2004. The annual effective dose from natural sources of ionising radiation in Canada. Radiat. Protect. Dosim. 108 (3), 215–226.

Hurtado, S., et al., 2004. GEANT4 code for simulation of a germanium gamma-ray detector and its application to efficiency calibration. Nucl. Instrum. Methods Phys. Res. A518, 764–774.

ICRP, 1996. Conversion Coefficients for Use in Radiological Protection against External Radiation. ICRP Publication 74. Ann. ICRP 26, 3-4.

ICRP, 1997. General principles for the radiation protection of workers. ICRP publication 75. Ann. ICRP 27 (1).

ICRP, 2020. Dose coefficients for external exposures to environmental sources. ICRP Publication 144. Ann. ICRP 49 (2).

ICRU, 1992. Measurement of Dose Equivalents from External Photon and Electron Radiations. ICRU report 47. International Commission on Radiation Units & Measurements.

ICRU, 2020. Operational Quantities for External Radiation Exposure. ICRU Report 95. International Commission on Radiation Units & Measurements.

IEC 61017, 2016. Radiation Protection Instrumentation – Transportable, Mobile or Installed Equipment to Measure Photon Radiation for Environmental Monitoring. Geneva, Switzerland.

IEC 60532, 2010. Radiation Protection Instrumentation - Installed Dose Rate Meters, Warning Assemblies and Monitors - X and Gamma Radiation of Energy between 50 keV and 7 MeV. Geneva, Switzerland.

Isaksson, M., 2011. Environmental Dosimetry Measurements and Calculations. Radioisotopes–Applications in Physical Sciences. InTech, ISBN 978-953-307-510-5. https://doi.org/10.5772/22731.

ISO 18589-7, 2013. Measurement of Radioactivity in the Environment - Soil - Part 7: in Situ Measurement of Gamma-Emitting Radionuclides. International Organization forStandardization, Geneva, Switzerland.

ISO 4037-1, 2019. Radiological protection - X and gamma reference radiation for calibrating dosemeters and doserate meters and for determining their response as a function of photon energy - Part 1: Radiation characteristics and production methods. International Organization for Standardization, Geneva, Switzerland.

ISO 4037-2, 2019. Radiological Protection - X and Gamma Reference Radiation for Calibrating Dosemeters and Doserate Meters and for Determining Their Response as a Function of Photon Energy - Part 2: Dosimetry for Radiation Protection over the Energy Ranges from 8 keV to 1,3 MeV and 4 MeV to 9 MeV. International Organization for Standardization, Geneva, Switzerland.

ISO 4037-3, 2019. Radiological Protection - X and Gamma Reference Radiation for Calibrating Dosemeters and Doserate Meters and for Determining Their Response as a Function of Photon Energy - Part 3: Calibration of Area and Personal Dosemeters and the Measurement of Their Response as a Function of Energy and Angle of Incidence. International Organization for Standardization, Geneva, Switzerland.

Kawrakow, I., et al., 2017. The EGSnrc Code System: Monte Carlo Simulation of Electron and Photon Transport. Technical Report PIRS-701. National Research Council Canada.

Liu, C., et al., 2018. Development of a national cosmic-ray dose monitoring system with Health Canada's Fixed Point Surveillance network. J. Environ. Radioact. 190–191, 31–38.

Liu, C., et al., 2019. Observation of ground-level enhancement across Canada's fixed point surveillance network during the 20 january 2005 solar event. Health Phys. 117 (3), 291–299.

Liu, C., Benotto, M., Ungar, K., Chen, J., 2022. Environmental monitoring and external exposure to natural radiation in Canada, 2022 J. Environ. Radioact. 243, 106811.

Moriuchi, S., Miyanaga, I., 1966. A spectrometric method for measurement of low-level gamma exposure dose, 1966 Health Phys. 12 (4), 541–551.

Ohera, Marcel, et al., 2020. Calibration of spectrometric detectors for air kerma rates in environmental monitoring. Nucl. Technol. Radiat. Protect. 35, 323–330. https://doi.org/10.2298/NTRP2004323O.

Radiation Solutions, 2021. Radiation Solution Inc. Website. https://www.radiationsolutions.ca/environmental/.

Saito, K., Moriuchi, S., 1981. Monte Carlo calculation of accurate response functions for a NaI(Tl) detector for gamma rays, 1981 Nucl. Instrum. Methods 185, 299–308.

Saito, K., Moriuchi, S., 1987. Data Catalog of Gamma Ray Response Functions for NaI(Tl) Scintillation Detectors by the Monte Carlo Calculation. JAER Report 9714, Tokai, Japan.

Tsuda, S., Saito, K., 2017. Spectrum-dose conversion operator of NaI(Tl) and CsI(Tl) scintillation detectors for air dose rate measurement in contaminated environments, 2017 J. Environ. Radioact. 166, 419–426.

Yi, C.Y., et al., 1997. Measurement of ambient dose equivalent using a NaI(Tl) scintillation detector. Radiat. Protect. Dosim. 74 (4), 273–278.

Zhang, W., et al., 2013. Testing of an automatic outdoor gamma ambient dose-rate surveillance system in Tokyo and its calibration using measured deposition after the Fukushima nuclear accident. J. Environ. Radioact. 125, 93–98.